

The modelling of nucleophilic and electrophilic additions to organometallic complexes using molecular graphics techniques

Jacques Weber^{a,*}, Peter Fluekiger^a, Pierre-Yves Morgantini^a, Olivier Schaad^a,
Annick Goursot^b and Claude Daul^c

^aLaboratory of Computational Chemistry, University of Geneva, 30 quai Ernest Ansermet, 1211 Geneva 4, Switzerland

^bNational School of Chemistry, 8 rue de l'Ecole Normale, 34075 Montpellier Cedex, France

^cInstitute of Inorganic Chemistry, University of Fribourg, Boulevard de Pérolles, 1700 Fribourg, Switzerland

Key words: Intermolecular interactions; Extended Hückel; Dot surfaces; Molecular properties; Reactivity

SUMMARY

A new formalism has been developed in order to evaluate intermolecular interaction energies for inorganic and organometallic complexes in the framework of the extended Hückel method. In order to provide the shortest possible response time on an interactive computer graphics facility, this model should require the minimum amount of computer time, which explains why approximate procedures are used to evaluate electrostatic, charge transfer and exchange repulsion components. When applying this model to typical examples of electrophilic addition reactions to organometallic complexes, it is found that it is essential to take account of charge transfer interactions, the electrostatic component alone being not sufficient, even qualitatively, for a proper description of the reaction mechanism. The results, presented as color-coded dot molecular surfaces, show a very good agreement with experiment as to the site of attack, namely (i) on metal for the electrophilic attack on $\text{Fe}(\text{cp})_2$, $\text{Fe}(\text{CO})_5$ and $\text{X}(\text{cp})(\text{CO})_2$, $\text{X} = \text{Co}, \text{Rh}$; (ii) on the cp ligand for the nucleophilic attack on $\text{Co}(\text{cp})_2^+$ and $\text{Rh}(\text{cp})_2^+$; (iii) on bz for the nucleophilic attack on $\text{Fe}(\text{cp})(\text{bz})^+$. Finally, modellizations of the nucleophilic attack on a coordinated olefin and of the relation between structure and acidic properties of zeolites are presented and discussed.

INTRODUCTION

Nucleophilic, and to a lesser extent electrophilic, addition reactions are essential reaction mechanisms in catalytic processes involving organometallic complexes [1–3]. Indeed, coordination to a metal atom may significantly change the charge distribution within a given organic ligand, resulting in considerable activation of specific sites which may then undergo nucleophilic or electrophilic attack. Various approximate models, based on molecular orbital (MO) theory, are commonly

* To whom correspondence should be addressed.

used in order to interpret, and possibly predict, the main features of such addition reactions: they are generally based on (i) an analysis of the frontier orbitals of the transition metal (TM) complex, perturbed by the appropriate orbitals of the attacking reactive [4–6]; or (ii) a calculation of the interaction energy between the TM complex and the reactive, with the different energy components approximated by various techniques such as multipolar expansion or second-order perturbation [7–9]. Although in the last few years some partial ab initio SCF (and in some cases CI) studies of the mechanisms associated with nucleophilic attack on organometallic complexes have been reported [10–12], the amount of computer time these techniques require for investigating these reactions is still very important and generally necessitates the use of supercomputers.

On the other hand, considering the spectacular development of molecular graphics (MG) techniques, we felt that it was time to combine an approximate MO treatment of these reactions with the most recent graphics techniques in order to enable the chemist to rapidly evaluate and visualize their main characteristics, such as the sites of attack, interaction energies, activation barriers, etc. In our opinion, this new tool should be based on a theoretical model as simple as possible, though leading to meaningful results, so as to achieve the qualitative modellization of a simple reaction within a very short response time, typically of the order of one minute on the PS 390 linked to a VAX 11/780. We have therefore chosen the extended Hückel (EH) method [13], which is able to reasonably predict in a very short time the electronic structure of TM complexes, and decided to develop a new formalism for evaluating intermolecular interaction energies within this model.

Basically, intermolecular energies are made of the following components: electrostatic, charge transfer, polarization, dispersion and exchange repulsion. For TM complexes, the first two terms undoubtedly predominate. In our model, the electrostatic energy is approximated by the molecular electrostatic potential (MEP) of the unperturbed substrate (i.e. the TM complex itself) calculated within the EH framework using novel procedures. The charge transfer component is readily approximated using EH total energies calculated for the fragments and the supermolecule. Exchange repulsion is taken into account in an approximate way by restraining the incoming reactive on the molecular surface of the substrate. Physically, this means that these effects have been described so far in our model by using simply an infinite vertical potential on the molecular surface, but in a next step this crude approximation is going to be replaced by a parametrized potential. In addition, work is in progress in order to evaluate the polarization and dispersion components by approximate techniques.

In this paper, the theoretical model we propose will be described and preliminary results will be presented. The reactions studied so far, and used as test cases for our model, are typical examples of organometallic reactivity: protonation of ferrocene and iron pentacarbonyl; electrophilic attack on the half-sandwich complexes: $X(cp)(CO)_2$, $X=Co,Rh$; nucleophilic attack on $X(cp)_2^+$, $X=Co,Rh$; nucleophilic attack on $Fe(cp)(bz)^+$ and on an olefin coordinated to $Pd(II)Cl_3^-$; acidic properties of zeolites. In each case, the theoretical results will be presented as two-dimensional (2D) contour maps or 3D colored dot molecular surfaces of interaction energies, which will enable us to discuss and compare them with experimental evidence.

THEORETICAL MODEL

In the present work, interaction energies E_{int} are expressed as:

$$E_{int} = E_{es} + E_{ct} + E_{ex} \quad (1)$$

where E_{es} , E_{ct} and E_{ex} stand for electrostatic, charge transfer and exchange repulsion components, respectively.

In order to display reactivity maps, E_{int} is evaluated repeatedly at selected points located in a planar grid (2D) or on the Connolly surface [14] (3D representation) of the substrate S. The external reactive R is modelled as a proton with an empty 1s orbital (electrophilic attack) and an H^- hydride ion with two electrons in a 1s orbital (nucleophilic attack). In both cases, R is spherically symmetric, which considerably facilitates the evaluation of E_{int} .

Electrostatic and exchange repulsion components

According to Scrocco and Tomasi [15], the electrostatic interaction energy of a positive point charge, located in \mathbf{r} , with an undistorted substrate is given within the LCAO framework by:

$$V^e(\mathbf{r}) = \sum_A \frac{Z_A}{|\mathbf{r} - \mathbf{r}_A|} - \sum_{\mu, \sigma} P_{\mu\sigma} \left\langle \mu \left| \frac{1}{|\mathbf{r} - \mathbf{r}'|} \right| \sigma \right\rangle \quad (2)$$

where the first term corresponds to nuclear repulsion, the summation running over all atoms A of S, with nuclear charge Z_A and located in \mathbf{r}_A . The second term originates from the electronic attraction, $P_{\mu\sigma}$ being the first-order density matrix element corresponding to atomic orbitals (AOs) μ and σ , and $\left\langle \mu \left| \frac{1}{|\mathbf{r} - \mathbf{r}'|} \right| \sigma \right\rangle$ being defined as:

$$\left\langle \mu \left| \frac{1}{|\mathbf{r} - \mathbf{r}'|} \right| \sigma \right\rangle = \int \chi_\mu(\mathbf{r}') \frac{1}{|\mathbf{r} - \mathbf{r}'|} \chi_\sigma(\mathbf{r}') d\mathbf{r}' \quad (3)$$

This integral, written more conveniently as $\langle \mu | 1/r | \sigma \rangle$, represents the electrostatic attraction between an electron located in AOs $\chi_\mu \chi_\sigma$ and the incoming proton. In our model, $V^e(\mathbf{r})$ is the MEP of the substrate and it corresponds to E_{es} for the electrophilic attack. In addition, as the model electrophile has no electrons, the exchange component E_{ex} vanishes.

In the case of a nucleophilic addition reaction, the electrostatic interaction $V^n(\mathbf{r})$ between S and R is approximated in our case by depicting R as a negative point charge, which leads to the following expression:

$$V^n(\mathbf{r}) = - \sum_A \frac{Z_A}{|\mathbf{r} - \mathbf{r}_A|} + \sum_{\mu, \sigma} P_{\mu\sigma} \langle \mu | 1/r | \sigma \rangle \quad (4)$$

Furthermore, the exchange repulsion potential $E_{ex}(\mathbf{r})$ can be approximated as [8]:

$$E_{ex}(\mathbf{r}) = C k_{nucl} \sum_A k_A \exp \left[- \frac{\alpha |\mathbf{r} - \mathbf{r}_A|}{R_{OA}} \right] \quad (5)$$

where C is a universal constant; k_{nucl} and k_A are parameters depending on nucleophile and atom

A , respectively; $R_{OA} = 2(R_A R_{\text{nucleophile}})^{1/2}$, R_A and $R_{\text{nucleophile}}$ being parameters describing the size of atom A and of nucleophile, respectively; α is a dimensionless constant usually taken as 12.35. In our model, $V^n(r)$ corresponds therefore to E_{es} for the nucleophilic attack. As mentioned earlier, $E_{ex}(r)$ will be approximated in these preliminary calculations by an infinite potential at the Connolly surface.

In the EH model, atomic orbitals are of Slater type, which makes the calculation of $\langle \mu | 1/r | \sigma \rangle$ integrals difficult and time consuming. We propose thus two different schemes so as to reduce the number of these integrals.

The first one is based on the neglect of diatomic differential overlap (NDDO) approximation [16]. In this scheme, all the integrals $\langle \mu | 1/r | \sigma \rangle$ with μ and σ belonging to different atoms vanish, which leads to the following expression for the second right-hand term of Eq 2:

$$\sum_A \sum_{\mu \in A} P_{\mu \sigma_A} \langle \mu_A | 1/r | \sigma_A \rangle \quad (6)$$

the first summation running over all the atoms A of the substrate. However, the evaluation of the reduced density matrix elements $P_{\mu \sigma_A}$ has to be performed using orthogonalized atomic basis functions in order to ensure that

$$\text{Trace} \{ P_{\mu \sigma_A} \} = N \quad (7)$$

where N is the number of valence electrons of the molecule. Using the Löwdin orthogonalization procedure [17], the density matrix elements $P_{\mu \sigma_A}$ are then given by the formula:

$$P_{\mu \sigma_A} = \sum_i n_i \sum_{\lambda, \rho} c_{\lambda i} S_{\mu \lambda}^{1/2} S_{\sigma \lambda}^{1/2} c_{\rho i} \quad (8)$$

where n_i is the occupation number of the i th molecular orbital (MO); $c_{\lambda i}$ is the coefficient of the i th MO corresponding to the λ -th AO and $S_{\mu \lambda}^{-1/2}$ is a symmetric square matrix such that

$$S_{\mu \sigma} = \sum_{\lambda} S_{\mu \lambda}^{-1/2} S_{\sigma \lambda}^{-1/2} \quad (9)$$

$S_{\mu \sigma}$ being the overlap between AOs μ and σ . It is then easy to prove that Eq. 7 is verified using Eq. 8 for $P_{\mu \sigma_A}$.

The second scheme leading to a reduction of the number of $\langle \mu | 1/r | \sigma \rangle$ integrals of Eq. 2 is based on the use of Mulliken approximation [18]:

$$\langle \mu | 1/r | \sigma \rangle = 1/2 S_{\mu \sigma} [\langle \mu | 1/r | \mu \rangle + \langle \sigma | 1/r | \sigma \rangle] \quad (10)$$

which, as shown by Carbo and Martin [19], leads to the following expression for the electronic part of Eq. 2:

$$\sum_{\mu,\sigma} P_{\mu\sigma} \langle \mu | 1/r | \sigma \rangle = \sum_{\mu} D_{\mu} \langle \mu | 1/r | \mu \rangle \quad (11)$$

with D_{μ} , the gross orbital population of AO μ , given by $D_{\mu} = \sum_{\sigma} P_{\mu\sigma} S_{\mu\sigma}$.

Eq. 6 and 10 show that it is straightforward to evaluate MEPs from EH wave functions, the only difficulty lying in the calculation of $\langle \mu | 1/r | \sigma \rangle$ integrals over Slater functions. In a forthcoming paper, this latter point will be developed in more detail [20].

In the next Section, the MEP calculated in the NDDO scheme will be designated as MEP(I), whereas that evaluated using the Mulliken approximation will be called MEP(II).

Charge transfer component

In our model, the electronic structure of R is described by a single atomic orbital in both cases of electrophilic and nucleophilic attack. This allows to write, within the Wolfsberg–Helmholz framework [21], the effective Hamiltonian for the S–R interaction as:

$$\langle \varphi_i^S | H | \varphi^R \rangle = 1/2 K S_i (\epsilon_i + H_R) = h_i \quad (12)$$

where φ_i^S is the i th MO of S, with energy ϵ_i , φ^R and H_R are the AO and Coulomb energy of R, respectively, S_i is the overlap integral between φ_i^S and φ^R , K is the Wolfsberg–Helmholz constant chosen as 1.75. The one-electron energies and wave functions of the S–R supermolecule are then obtained from the secular equations:

$$\begin{bmatrix} \epsilon_1 & & & \\ \epsilon_2 & \ddots & & \\ \epsilon_3 & & 0 & \\ & & & \ddots \\ & & & 0 \\ & & & & \epsilon_n & h_n \\ & & & & h_1 & h_2 & \dots & h_n & H_R \end{bmatrix} C = \begin{bmatrix} 1 & & & & & \\ & 1 & & & & \\ & & 1 & & & \\ & & & 0 & & \\ & & & & 0 & \\ & & & & & \ddots \\ & & & & & & 0 \\ & & & & & & & \ddots \\ & & & & & & & & 0 \\ & & & & & & & & & 1 \\ & & & & & & & & & & S_1 \\ & & & & & & & & & & S_2 \\ & & & & & & & & & & \vdots \\ & & & & & & & & & & \vdots \\ & & & & & & & & & & S_n \\ & & & & & & & & & & 1 \\ & & & & & & & & & & S_n \end{bmatrix} \quad CE \quad (13)$$

Solving Eq. 13 is rather time consuming as it requires in principle the diagonalization of a large supermatrix. However, when the distance between R and the substrate becomes long enough, it is possible to use second-order perturbation theory in order to solve this system, which leads to a considerable reduction in computer time.

As EH total energies represent roughly the sum of covalent energies within chemical bonds, E_{ct} may be approximated as

$$E_{ct} = E^{tot}(SR) - E^{tot}(S) - E^{tot}(R) \quad (14)$$

where $E^{\text{tot}}(X)$ represents the EH total energy of system X calculated as:

$$E^{\text{tot}}(X) = \sum_i n_i \varepsilon_i \quad (15)$$

where n_i and ε_i are occupation number and energy, respectively, of the i th MO of X.

$E_{\text{ct}}(\mathbf{r})$ is then readily obtained by solving Eq. 13 and using Eq. 14 for the SR^+ (electrophilic attack) or SR^- (nucleophilic attack) system for different positions of the reactive R. Actually, this approximation of the charge transfer component is very similar to that proposed by Brown et al. [21].

Two-body correction

Anderson has suggested to add a two-body repulsive correction (2BC) to EH total energies in order to improve the results of the model for structure and reactivity predictions [22]. As this procedure amounts approximately to the introduction of electrostatic effects, an alternative method to calculate interaction energies is to add this two-body correction to E_{ct} , and we found it worthwhile to test this correction for some standard addition reactions. In our case, the two-body correction E_{2BC} writes as follows:

$$E_{\text{2BC}}(\mathbf{r}) = \sum_A \left[\frac{Z_A}{|\mathbf{r} - \mathbf{r}_A|} - \int \frac{\rho_A(\mathbf{r}')}{|\mathbf{r} - \mathbf{r}'|} d\mathbf{r}' \right] \quad (\text{electrophilic attack}) \quad (16a)$$

$$E_{\text{2BC}}(\mathbf{r}) = \sum_A \left[\frac{Z_A}{|\mathbf{r} - \mathbf{r}_A|} - \int \frac{\rho_n(\mathbf{r}' - \mathbf{r})}{|\mathbf{r}_A - \mathbf{r}'|} d\mathbf{r}' \right] \quad (\text{nucleophilic attack}) \quad (16b)$$

where the summations run over the atoms of the substrate; Z_A , \mathbf{r}_A and ρ_A are the nuclear charge, position and electronic density of atom A, respectively; \mathbf{r} is the position of the reactive and ρ_n the electronic density of the nucleophile.

Whereas the first term of the right-hand side of Eqs. 16a and 16b represents the electrostatic interaction between the nucleus of R and all the nuclei of S, the second term has different meanings according to the nature of R. In Eq. 16a, it corresponds to the electrostatic interaction between the incoming acceptor and the electronic densities of all atoms A belonging to S. However, in Eq. 16b, it corresponds to the electrostatic interaction between the electronic density of the incoming donor and the nuclei of all atoms A belonging to S. Approximate expressions 16a and 16b represent therefore part of the electrostatic energy component for S-R interaction.

The integrals of the right-hand side of Eq. 16 are evaluated assuming spherical atomic charge densities. The alternative expression for interaction energies writes therefore:

$$E_{\text{int}}' = E_{\text{ct}} + E_{\text{2BC}} \quad (17)$$

Calculations and graphics

All the EH calculations have been performed on a VAX11/780 computer, using the self-consistent charge and configuration procedure with a quadratic dependence for the H_{ii} of metal, those of the other atoms being kept fixed. The standard set of EH parameters and atomic radial func-

tions has been used [23], the only exception being hydrogen for which a 1s exponent of 1.0 was chosen in order to improve the description of the reactive R.

2D contour maps were generated on an AED-512B raster scan color display and on a HP 7221A plotter using the IDC package [24]. For the 3D representation, a solvent-accessible molecular surface was first calculated according to the algorithm suggested by Connolly [14]. Interaction energies were then calculated at each surface point and subsequently displayed as colored dots on the Evans & Sutherland PS 390 using the MANOSK molecular modelling package [25]. Special coloring codes, defined and scaled by features of this package, were employed to achieve optimal color differentiation leading to the perception of MEP gradients over the Connolly surface. As it is possible with MANOSK to build and manipulate up to four independent molecules and surfaces, the interpretation and comparison of even minute details of these interaction energies is greatly facilitated.

RESULTS AND DISCUSSION

In order to compare in some detail the results obtained using the two procedures MEP(I) and MEP(II), Fig. 1 presents the variation of these properties with distance for several TM complexes. It is seen that in all the cases MEP(I) is lower (i.e. more negative) than MEP(II), lying generally at an intermediate position between MEP(II) and $\text{MEP(II)} + E_{ct}$ in the 1.0–2.5 Å range or at even lower energies than this latter property (zeolite). On the other hand, further investigations [26] have shown that for small molecules and TM complexes as well (see below), the MEPs calculated using the EH model and approximation II compare very well with those derived from ab initio SCF wave functions, the main features of MEPs contour maps being qualitatively the same in both models. In particular, the position of MEP minima, i.e. the sites of electrophilic attack in the electrostatic approximation, are predicted to be very similar in both methods, which suggests that EH could be an interesting alternative to Hartree–Fock for the evaluation of MEPs of large compounds.

As expected, examination of Fig. 1 reveals that charge transfer effects lead to a significant stabilization of interaction energies, the $\text{MEP(II)} + E_{ct}$ curves lying at lower energies than MEP(II) alone. This is particularly true for cases 1a, 1b and 1c, where MEP(II) shows no bonding in the vicinity of metal for the incoming proton whereas $\text{MEP(II)} + E_{ct}$ exhibits a deep minimum in each case. Taking as an example the case of ferrocene, this result is consistent with the observation that this compound protonates in solution on the metal atom [27–29]. On the other hand, when compared with MEP(II) , the behavior of MEP(I) is different as this property displays a large negative region along the OY axis, with a minimum lying at about 1.8 Å. This result, together with the observation that MEP(I) is constantly lower in energy than MEP(II) for all the TM complexes we have investigated, suggests that through the NDDO approximation MEP(I) includes to some extent an empirical treatment of charge transfer effects. Through Eq. 8, the orthogonalization procedure of the first-order density matrix performed before evaluating MEP(I) leads indeed to a reorganization of the electronic distribution within the molecule, a procedure which simulates somehow the charge transfer mechanism. It is therefore tempting to use MEP(I) as an approximation to $E_{es} + E_{ct}$ for both electrophilic and nucleophilic attacks and this procedure will be tested further on in this paper. However, the results of Fig. 1 demonstrate that in any case it is necessary to account for the E_{ct} component, or for a reasonable approximation of it, in order to properly de-

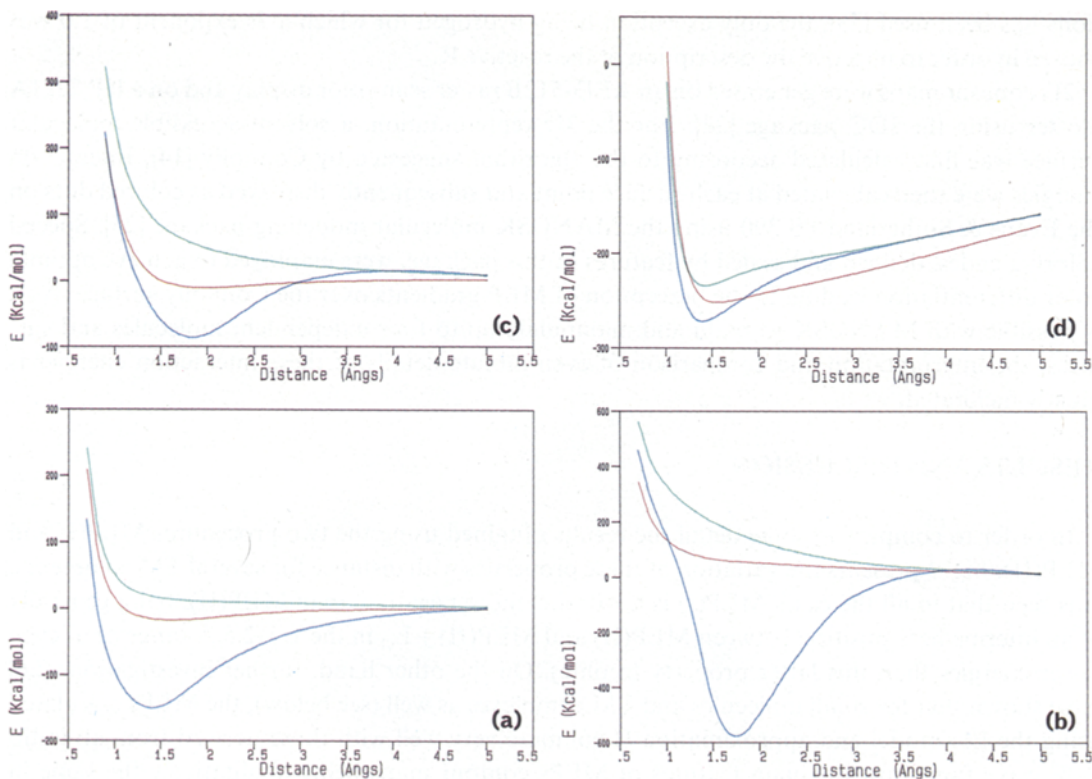
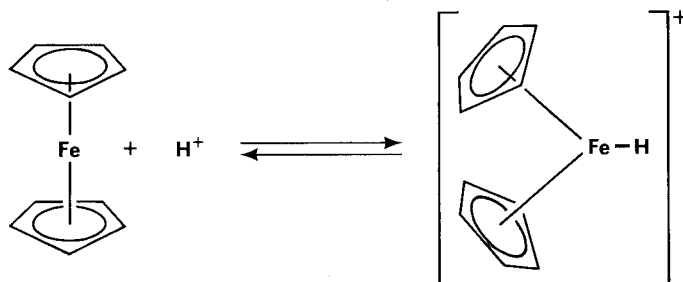


Fig. 1. Variation of interaction energies as a function of metal-reactive distance (the metal being located at origin) for the electrophilic attack in the following cases: (a) $\text{Fe}(\text{cp})_2$, the direction of attack being the OY axis (see Fig. 2); (b) $\text{Fe}(\text{CO})_5$, direction of the bisector of the C-Fe-C angle in the equatorial plane of the trigonal bipyramidal; (c) $\text{Rh}(\text{cp})(\text{CO})_2$, direction perpendicular to the $\text{Rh}(\text{CO})_2$ plane; (d) Al-Si-Si-Al zeolite, direction of central oxygen atom (O_z), along the bisector of the external $\text{T}_1-\text{O}_z-\text{T}_1$ angle (Fig. 9). In all cases, the color coding of the different curves is the following: red = MEP(I); green = MEP(II); blue = MEP(II) + E_{ct} .

scribe the mechanism of electrophilic attack in these complexes. The case of Al-Si-Si-Al zeolite (Fig. 1d) is different as the model compound used in this calculation bears a negative charge (-2), which automatically leads to a bonding electrostatic interaction with the incoming proton.



Scheme 1

The case of the protonation of ferrocene is particularly interesting as this compound has been used for a long time as a benchmark for quantum-chemical calculations, and this problem will now be discussed in some detail. From the experimental side, it is known according to NMR studies that ferrocene protonates readily in strong acids to give the reaction intermediate $\text{Fe}(\text{C}_5\text{H}_5)_2\text{H}^+$ [27, 28], the protonation site being located on metal, presumably in the equatorial

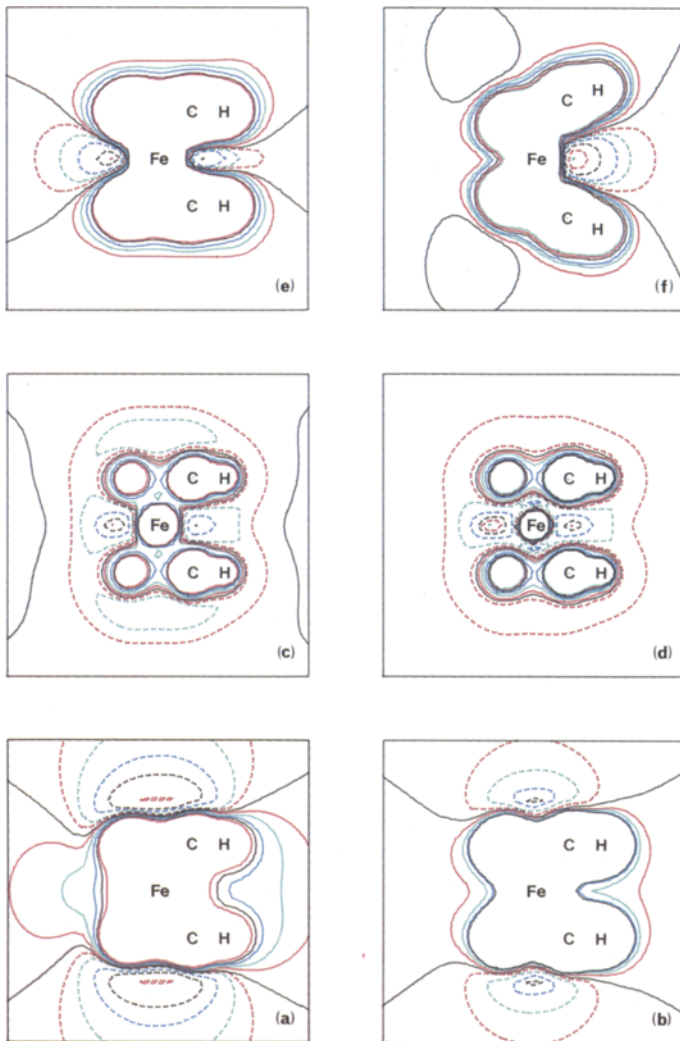


Fig. 2. Contour maps of interaction energies calculated for $\text{Fe}(\text{cp})_2$ and represented in the YOZ plane (the OZ axis is the five-fold symmetry axis and the OY axis lies in the equatorial plane, eclipsing one C-H bond of each cp ring). Positive (negative) contours are indicated by a solid (dashed) line. (a) ab initio MEP, minimum at -43 kcal/mol ; (b) EH MEP(II), min. at -17 kcal/mol ; (c) EH MEP(II) + E_{ct} , min. at -147 (right) and -179 (left) kcal/mol ; (d) EH $E_{2BC} + E_{ct}$, min. at -160 (right) and -185 (left) kcal/mol ; (e) EH MEP(I), min. at -18 (right) and -22 (left) kcal/mol ; (f) EH MEP(I) of ring-tilted $\text{Fe}(\text{cp})_2$ ($\text{cp-Fe-cp angle: } 140^\circ$), min. at -42 kcal/mol .

plane. In addition, $\text{Fe}(\text{C}_5\text{H}_5)_2\text{H}^+$ exhibits a tilted ring structure, with the proton oriented in the direction of the sandwich opening [30] (Scheme 1).

It is therefore anticipated that the theoretical models will lead to interaction energies for the $\text{Fe}(\text{C}_5\text{H}_5)_2 + \text{H}^+$ reaction exhibiting a minimum on metal. Figure 2 presents contour levels of these interaction energies calculated using both Hartree-Fock and EH models at different levels of approximation. Comparing Figs. 2a and b, it is immediately seen that the ab initio Hartree-Fock and EH (case II) MEPs are very similar, both displaying no protonation site on metal as the contour levels are positive everywhere in the vicinity of the iron atom. On the other hand, large negative potentials are observed extending beyond the cp rings in the outer π region, with minima located approximately above the center of the rings, as is the case for the free C_5H_5^- anion. According to these MEPs, ferrocene would therefore protonate on the π ligand rings, which is not consistent with NMR experiments. Clearly, an interaction energy based on the electrostatic component alone is not a sufficient model for describing the protonation of ferrocene, as could already be inferred from Fig. 1a. Introduction of CT effects within the EH framework leads to a significant improvement, as can be seen from Fig. 2c which displays the contour levels of $\text{MEP}(\text{II}) + E_{ct}$. Indeed, in agreement with experiment, minima of this interaction energy are now found on metal along the $+OY$ and $-OY$ axis of the equatorial plane. In addition, examination of Fig. 2c indicates that they correspond to much lower energies than those of the outer ring minimum, which confirms that this model actually predicts that ferrocene protonates on metal.

These results underline the importance of CT interactions in the equatorial plane of ferrocene, basically due to metal d_{xy} and $d_{x^2-y^2}$ electrons, as they drastically modify the picture which emerged from electrostatic effects alone. Interestingly, a similar conclusion may be drawn from ab initio results. Calculating separately E_{es} , E_{ct} and E_{pol} , the polarization energy, and expressing E_{int} as $E_{int} = E_{es} + E_{ct} + E_{pol}$, two minima are found: at 1.54 Å from metal along the $+OY$ axis and at 2.89 Å from metal along the OZ axis. At the minima, the E_{es} , E_{ct} and E_{pol} components have the following values: +73.1, -140.0 and -43.0 kcal/mol (OY axis) and -34.2, -41.8 and -23.0 kcal/mol (OZ axis), respectively, which leads to E_{int} values of -110.0 (OY) and -99.0 (OZ) kcal/mol. Though the latter values are much lower than the experimental proton affinity of ferrocene (213 kcal/mol) measured in gas phase by Foster and Beauchamp [29], they confirm that this compound protonates on metal because of predominant CT interactions.

Looking now at the possibility to substitute E_{es} by E_{2BC} in E_{int} suggested by Eq. 17, Fig. 2d presents the contour levels of $E_{int}' = E_{ct} + E_{2BC}$ calculated for ferrocene. The similarity with Fig. 2c, i.e. $E_{es} + E_{ct}$, is striking, which suggests that E_{2BC} could be used as an alternative for $\text{MEP}(\text{II})$. Finally, the performance of $\text{MEP}(\text{I})$ is illustrated in Fig. 2e, where one notices important differences with Fig. 2b ($\text{MEP}(\text{II})$). As mentioned above, there is little doubt that a partial simulation of CT effects is present in $\text{MEP}(\text{I})$ since the site of attack is now clearly on metal, which could not be obtained in the purely electrostatic approximation. However, the depth of the $\text{MEP}(\text{I})$ minimum (about -20 kcal/mol) is much higher than that predicted by $\text{MEP}(\text{II}) + E_{ct}$, which indicates that $\text{MEP}(\text{I})$ results are only of qualitative value. Opening the $\text{Fe}(\text{cp})_2$ sandwich, i.e. tilting the ring structure, leads obviously to a significant increase in metal basicity, as may be inferred from Fig. 2f. Indeed, the minimum of $\text{MEP}(\text{I})$ decreases to -42 kcal/mol for a ring tilt angle of 20°, i.e. a cp-Fe-cp angle of 140°, which emphasizes the importance of this structural deformation of the basicity. These results are in complete agreement with both the NMR study of Lentzner and Watts performed on [2]ferrocenophane [30] and previous EH calculations on $M(\text{cp})_2\text{H}^+$ complexes reported by Lauher and Hoffmann [31].

After these 2D representations of interaction energies, it is time to turn to 3D models, which should be more spectacular and informative, specially for large molecules with low symmetry. However, we should keep in mind that, especially in the case of electrophilic attack ($E_{ex}=0$), the colored dot Connolly surface does not in general represent the most reactive sites of the substrate, which actually correspond to absolute minima of E_{int} , but only the relative reactivity of a selected number of points belonging to the surface. In cases where protonation sites (i.e. absolute minima) are located at some distance from the surface, this representation could therefore be misleading.

Figure 3 displays the molecular surface of ferrocene represented as color-coded dots corresponding to the various interaction energies discussed in this paper. As expected, this type of representation is more informative as it allows to visualize the 3D features of the interaction energies, such as the five-fold symmetry around the OZ axis, whereas both clipping and depth-cueing facilities lead to a clear identification of the various parts of the surface. For ferrocene, the same trends as deduced from 2D contour levels are easily observed: $MEP(II)+E_{ct}$ and $E_{2BC}+E_{ct}$ (Fig. 3b) have remarkably similar features over the whole surface, whereas, in the case of $MEP(I)$ (Fig. 3a), the large red zone appearing around the OY axis in the region of the ring opening clearly reveals an increase in metal basicity and consequently in reactivity towards the incoming electrophile.

Iron pentacarbonyl protonates in strong acid solutions only, revealing a rather low basicity, to give the $Fe(CO)_5H^+$ compound with the proton directly bound to metal [32, 33]. Its reactivity towards electrophilic attack is therefore similar to that of ferrocene, though $Fe(CO)_5$ exhibits a slightly smaller proton affinity in gas phase (204 kcal/mol) [33]. As for $Fe(cp)_2$, it is expected that CT effects will play a predominant role in the theoretical description of the protonation of $Fe(CO)_5$, especially in favoring the site on metal. Examination of Fig. 4 shows indeed that the MEP approximation, even within the NDDO formalism which apparently includes some CT, predicts protonation on the oxygen atoms of the carbonyl groups, which can be easily understood on the basis of the large electron density associated with the lone pairs of oxygen atoms. A similar result has been obtained previously using the MEP calculated from ab initio wave functions [26]. However, introduction of CT effects changes drastically the electrostatic picture as Fig. 4 reveals that $MEP(II)+E_{ct}$ leads to strongly negative regions around the iron atom, at positions corresponding roughly to the lobes of d_{xz} and d_{yz} orbitals. Mostly because they lie at higher energies, the occupied d orbitals of metal are better σ donors than the lone pairs of oxygen, which leads to more negative values of E_{ct} (and also of E_{int}) in the metal region than around oxygen atoms. In this case again, introduction of CT interactions is essential in order to describe adequately the mechanism of electrophilic attack.

Werner has shown that half-sandwich complexes of general formula $C_nR_nML_2$, where M is a d⁸ transition metal, behave as Lewis bases and react with a large number of electrophiles, the addition taking place on metal [34]. In particular, $Co(cp)(CO)_2$ and $Rh(cp)(CO)_2$ react with HgX_2 ($X=Cl, Br, I$) to give the donor-acceptor complexes $M(cp)(CO)_2HgX_2$ containing a direct metal-mercury bond [35, 36]. It was therefore interesting to test further our model by choosing these two examples and the results are presented in Fig. 5. It is seen that indeed the red zones indicating the most negative regions of the $MEP(II)+E_{ct}$ interaction potential are located around the metal atom and not on the carbonyl groups, whereas the opposite picture had been again predicted on the basis of MEPs alone. When comparing the results obtained for the two compounds, the cobalt complex exhibits a minimum interaction energy on the Connolly surface which is about 115 kcal/

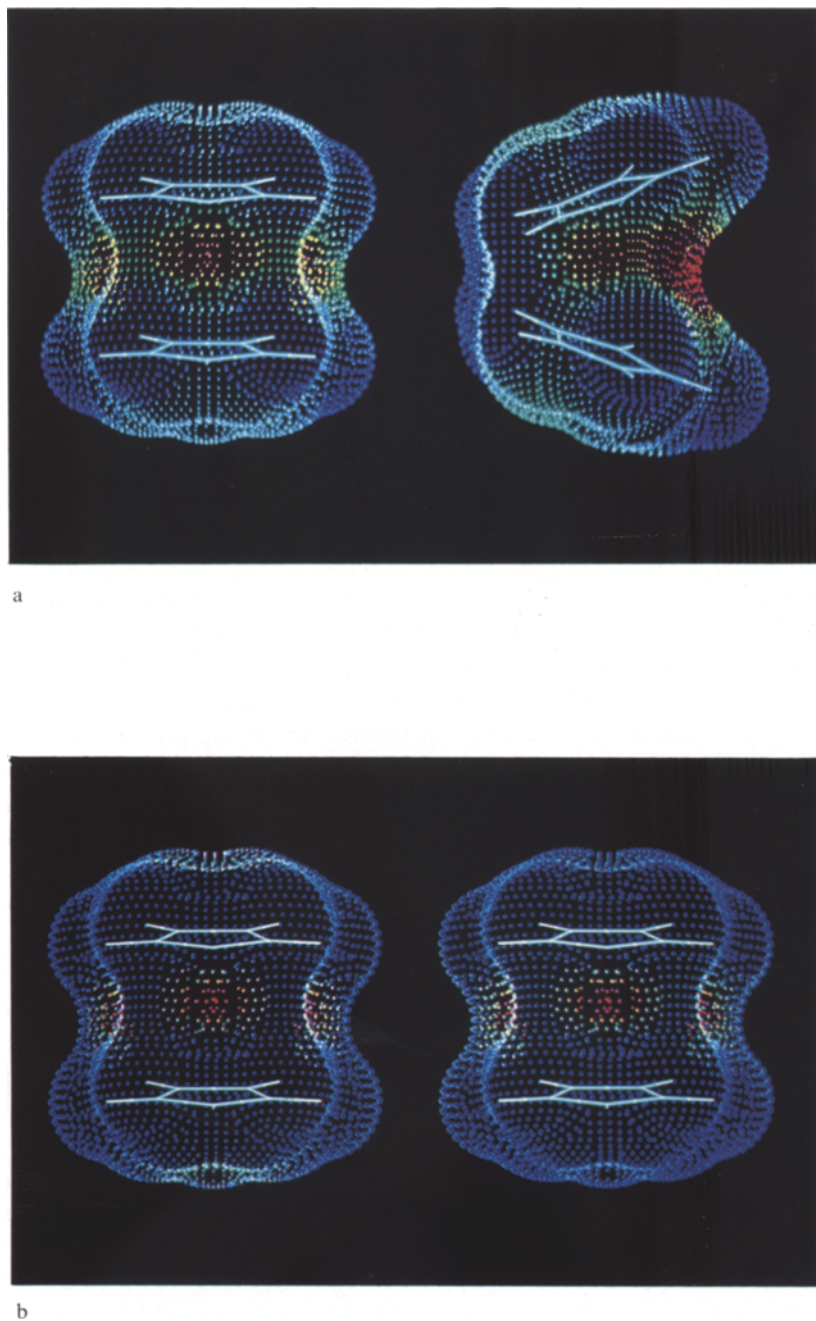


Fig. 3. (a) Color-coded representation of MEP(I) on the Connolly surface of $\text{Fe}(\text{cp})_2$ and ring-tilted $\text{Fe}(\text{cp})_2$ (cp-Fe-cp angle: 140°). The encoding of the interaction energy values is the same for all figures, i.e. the color range from red to yellow to blue extends smoothly over the numerical range of the property from most negative to neutral to most positive values. (b) Color-coded representation of $\text{MEP(II)} + E_{\text{ct}}$ (left) and $E_{2\text{BC}} + E_{\text{ct}}$ (right) on the surface of undistorted $\text{Fe}(\text{cp})_2$.

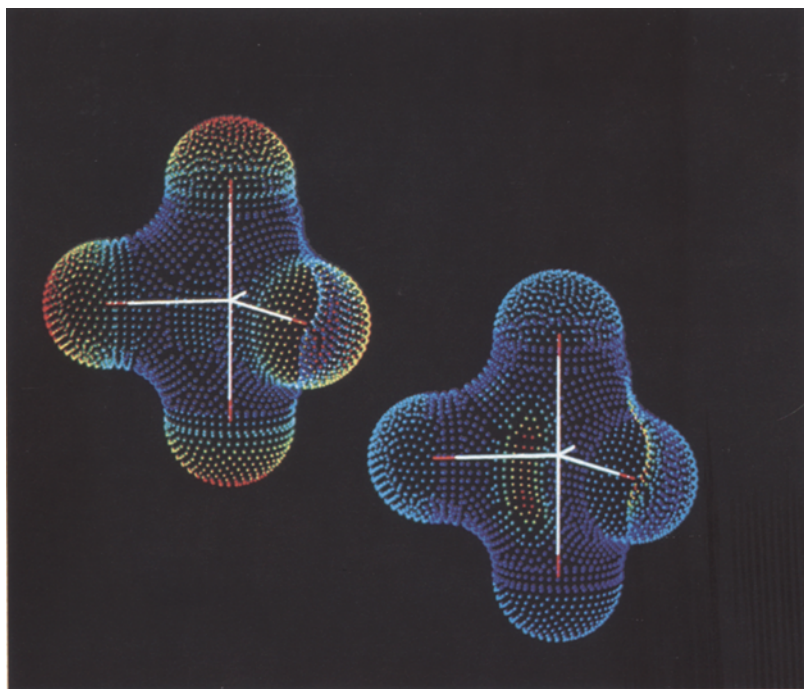


Fig. 4. Color-coded representation of MEP(I) (left) and MEP(II) + E_{ct} (right) on the surface of $\text{Fe}(\text{CO})_5$. The vertical OZ axis is the C_3 axis of the trigonal bipyramidal.

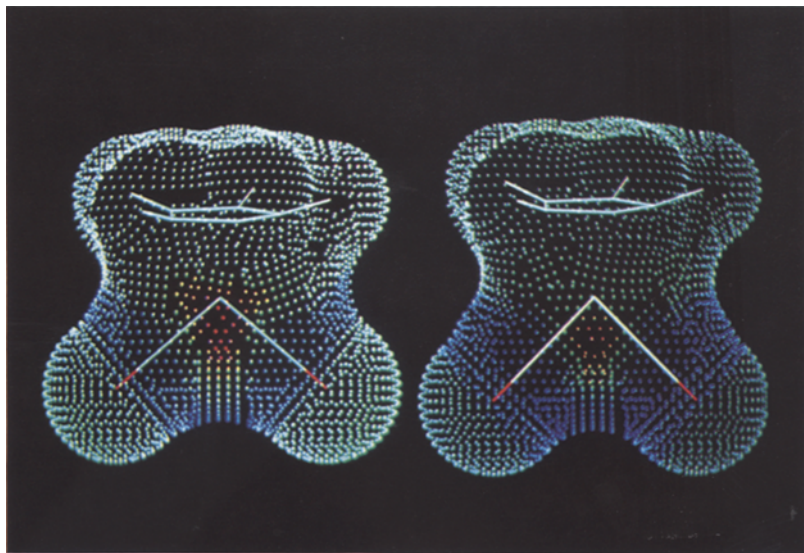


Fig. 5. Color-coded representation of MEP(II) + E_{ct} on the surface of $\text{Co}(\text{cp})(\text{CO})_2$ (left) and $\text{Rh}(\text{cp})(\text{CO})_2$ (right).

mol lower than that of the rhodium compound, whereas kinetic data for the species M(cp)-(CO)PPh₃ indicate that the metal basicity of cobalt should be similar to that of rhodium [34]. However, as mentioned above, negative values of interaction energies displayed on the Connolly surface may be different from absolute minima, as their variation as a function of metal-electrophile distance may be steep. In addition, the choice of van der Waals radii for metal atoms is rather arbitrary, which makes it difficult to compare quantitatively the values of interaction potentials on metal spheres.

Davies et al. [2] have proposed simple rules for rationalizing the most favorable positions of nucleophilic attack on 18 electron organometallic cations containing unsaturated hydrocarbon ligands. For cations which do not contain a coordinated CO, the nucleophilic attack invariably occurs on the exo-face of the ligand. Typical examples are Co(cp)₂⁺ and Rh(cp)₂⁺ for which the stereochemistry of the nucleophilic attack by lithium aluminum hydride has been studied by Green et al. [37] who conclude that the C₅H₆ ligand in Co(cp)₂H and Rh(cp)₂H exhibits an η^4 -bonding with the metal through the two double bonds of the diene system, the carbon atom of the methylene group being displaced out of the plane of the diene. Figure 6 represents the MEPs(I) calculated for Co(cp)₂⁺ and Rh(cp)₂⁺ on the Connolly surface. The most reactive sites for the nucleophilic attack are the blue regions located on the exo-face of the ligand rings, at the intersection of the OZ axis with the molecular surface. A complete description of the mechanism of nucleophilic attack would require of course to calculate an accurate reaction pathway, taking into account the important ligand distortion which accompanies the approach of the reactive, but it is rewarding that this simple model, using frozen geometries and approximate wave functions, is able to predict within a very short response time the most reactive site of the substrate. The same conclusion applies to the mixed sandwich compound Fe(cp)(bz)⁺, for which previous NMR [38] and theoretical [2] studies have shown that nucleophilic attack takes place exclusively on the exo-face of the benzene ligand. Examination of Fig. 7 shows that indeed, according to our model, the benzene ligand is much more reactive towards the incoming nucleophile, as one notices that the blue color of the region below the center of the bz ring is much darker than the corresponding zone above the cp ligand. Actually, the lowest interaction energies, which are found again at the intersection of the OZ axis with the surface, are -114 and -130 kcal/mol for the cp and bz rings, respectively, which leads to quite distinct reactivities easily visualized on the graphics system.

The reaction of an olefin with a TM complex is a basic process in homogeneous catalysis [1]. For example, whereas an unactivated olefin does not usually undergo nucleophilic attack, its coordination to a TM complex generally accelerates the reaction. To illustrate this mechanism, we have chosen the well-known case of the nucleophilic attack on an ethylene moiety coordinated to Pd(II)Cl₃⁻ [11, 12, 39]. PdCl₃⁻ is a square-planar complex with one vacant coordination site available for an incoming C₂H₄ ligand, which leads for PdCl₃(C₂H₄)⁻ to a structure analogous to that of the Zeise's anion [40], i.e. the C-C double bond of ethylene is perpendicular to the PdCl₃ plane. In order to confirm that a nucleophilic attack is more likely to take place on the coordinated ethylene than on an uncoordinated one (i.e. the so-called palladium-assisted mechanism), we have represented in Fig. 8 the MEPs(I) of both the PdCl₃(C₂H₄)⁻ complex and an isolated C₂H₄ molecule. It is seen that, as expected, the red zone of the interaction potential around the chlorine atoms reflects the propensity of this part of the complex to undergo an electrophilic attack, whereas the dark blue zone in the π region of coordinated ethylene is characteristic of a tendency towards nucleophilic attack. When comparing with the isolated C₂H₄ species, it is evident that the

blue color is lighter around the latter compound, which indicates a significantly reduced reactivity towards nucleophilic attack. Actually, there is a difference of 10 kcal/mol, in favor of the complex, between the most reactive regions around coordinated and free C₂H₄, which clearly confirms the acceleration of the reaction through coordination to the TM complex.

Finally, our last example will be devoted to the study of the acidic properties of zeolites of the offretite type. The modellization, using MG techniques, of several physicochemical properties of zeolites has been recently reviewed by Ramdas et al. [41] and we would like to concentrate here on another aspect of the unusual properties of these materials, namely the relation between structure and acidity or basicity in offretite. It is well known that the aluminosilicate framework of zeolites is made of corner-sharing SiO₄ and AlO₄ tetrahedra (Fig. 9) and Barthomeuf [42] observed that an important increase in offretite acid strength is concomitant with a decrease in the aluminum content of this zeolite framework. In other words, when achieving isomorphous substitutions of silicon by aluminum atoms, the basicity of the framework increases in measure as the Al/(Al+Si) ratio increases [43]. This property of zeolites of the offretite type can be easily rationalized and visualized using the MEP(I) interaction potential of four tetrahedra subunits of the offretite framework. Figure 10 represents the colored dot Connolly surface around two models of offretite: the so-called Si-Si-Al-Si structure (S1) where T₂ sites (Fig. 9) are occupied by silicium atoms and T₁ sites by one silicium and one aluminum atom, and the Al-Si-Si-Al model (S2) where T₂ sites accommodate aluminum and T₁ sites silicium, respectively. It is seen in Fig. 10 that the surface around structure S2, specially in the region above the central part of the model, displays large red zones revealing a deep interaction energy for an incoming electrophile, whereas the corresponding zones around model S1 are yellow, which indicates that the potential is less negative. Actually, the minimum of MEP(I) calculated for model S2 lies at -276 kcal/mol, whereas the corresponding value for model S1 is -221 kcal/mol, which clearly confirms that the basicity of the framework is dictated by the Al/(Al+Si) ratio of offretite, decreasing this ratio leading to a smaller basicity (and therefore to a larger acidity) of the material. In addition, further calculations also confirm the experimental observation that the stability and acidic properties of T₁ vs T₂ sites strongly depend upon both their central atom and particular structural features [43], which suggests that the present model could also be used to rationalize the properties of heterogeneous catalysts such as zeolites.

CONCLUSIONS AND PERSPECTIVES

In this study, several different schemes for evaluating approximate intermolecular interaction energies have been developed and tested for organometallics. When developing the different components of this model, we have placed the emphasis on the shortest response time for the user of an MG system and not on the quantitative accuracy of the results. We are indeed of the opinion that, though up-to-date MCSCF+CI models are undoubtedly of great utility for numerical predictions of TM structures and reactivities, provided one has ample computer time available on a supercomputer, they are of little value in routine MG applications where it is necessary to build within a few seconds appropriate models of organometallic structures and to estimate within a few minutes their stability and reactivity, with a subsequent visualization and manipulation of their molecular properties. To meet these latter criteria, we have found that a model of intermolecular interaction energies based on the EH formalism can be extremely useful, as the present results

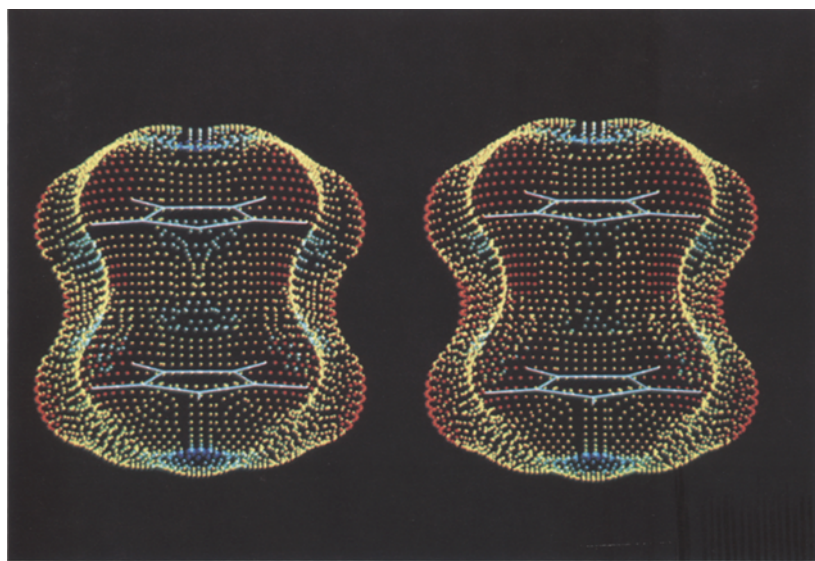


Fig. 6. Color-coded representation of $\text{MEP}(\text{I})$ on the surface of $\text{Co}(\text{cp})_2^+$ (left) and $\text{Rh}(\text{cp})_2^+$ (right). For the nucleophilic attacks, the interaction energies have been taken with the same sign as for an electrophilic attack: the encoding of energies is therefore the same as in Fig. 3, i.e. the most reactive regions for the nucleophilic attack are now in blue.

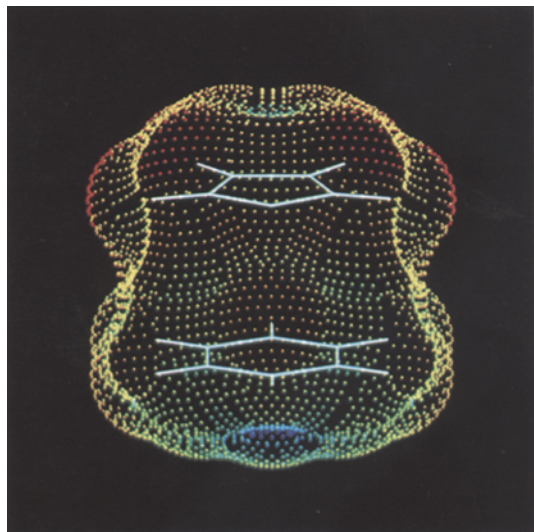


Fig. 7. Color-coded representation of $\text{MEP}(\text{I})$ on the surface of $\text{Fe}(\text{cp})(\text{bz})^+$.

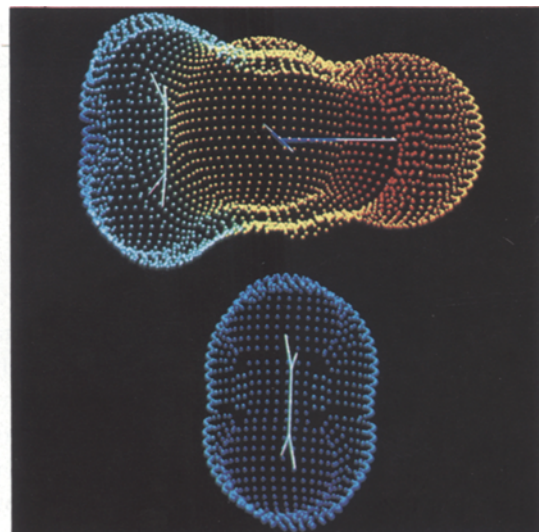


Fig. 8. Color-coded representation of $\text{MEP}(\text{I})$ on the surface of $\text{PdCl}_3(\text{C}_2\text{H}_4)^-$ (upper part) and C_2H_4 (lower part).

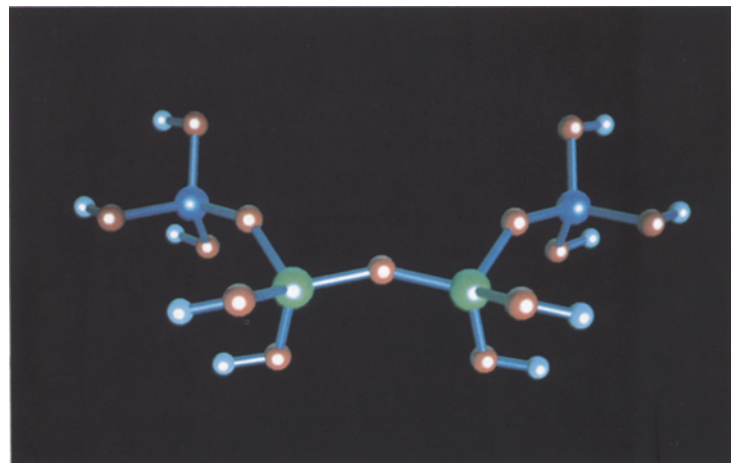


Fig. 9. Ball-and-stick model of the corner-sharing tetrahedra constituting the framework of zeolites of the offretite type, with T₁ (green balls) and T₂ (blue balls) inequivalent sites. Oxygen and hydrogen atoms are depicted by red and white balls, respectively.



Fig. 10. Color-coded representation of MEP(I) on the surface of Si-Si-Al-Si (upper part) and Al-Si-Si-Al (lower part) zeolites.

suggest that it can predict adequately reactivities towards electrophilic and nucleophilic attack, provided one introduces, even at a low level of approximation, charge-transfer interactions.

The present model is, however, at an early stage of development and much remains to be done so as to properly incorporate other effects such as polarization and dispersion. Another perspective would be to develop a model builder, much in the same way as such modules have been set up for building organic structures from fragments. However, this would require the development of parametrized force fields for inorganic and organometallic compounds, and the difficulties of such a prospect are real. Nevertheless, the possibilities of computer modelling and graphics are so broad that further developments along these lines will undoubtedly be pursued so as to fully extend the range of these techniques to inorganic and organometallic chemistry.

ACKNOWLEDGEMENT

This work is part of Project 2.806-0.85 of the Swiss National Science Foundation.

REFERENCES

- 1 Parshall, G.W. *Homogeneous Catalysis*, Wiley, New York, NY, 1980, p. 27.
- 2 Davies, S.G., Green, M.L.H. and Mingos, M.P., *Tetrahedron*, 34 (1978) 3047–3077.
- 3 Bäckvall, J.E., *Acc. Chem. Res.*, 16 (1983) 335–342.
- 4 Libit, L., and Hoffmann, R., *J. Am. Chem. Soc.*, 96 (1974) 1379–1383.
- 5 Fukui, K. and Inagaki, S., *J. Am. Chem. Soc.*, 97 (1975) 4445–4452.
- 6 Imamura, A. and Hirano, T., *J. Am. Chem. Soc.*, 97 (1975) 4192–4198.
- 7 Fukui, K. and Fujimoto, H., *Bull. Chem. Soc. Jpn.*, 41 (1968) 1989–1997.
- 8 Langlet, J., Claverie, P., Caron, F. and Boeuve, J.C., *Int. J. Quant. Chem.*, 20 (1981) 299–338.
- 9 Moriishi, H., Kikushi, O., Suzuki, K. and Klopman, G., *Theoret. Chim. Acta*, 64 (1984) 319–338.
- 10 Nakamura, S. and Dedieu, A., *Theoret. Chim. Acta*, 61 (1982) 587–595.
- 11 Bäckvall, J.E., Björkman, E.E., Petterson, L. and Siegbahn, P., *J. Am. Chem. Soc.*, 107 (1985) 7265–7267.
- 12 Sakaki, S., Moruta K. and Ohkubo K., *Inorg. Chem.*, 26 (1987) 2499–2505.
- 13 Hoffmann, R., *J. Chem. Phys.*, 39 (1963) 1397–1412.
- 14 Connolly, M.L., *Science*, 221 (1983) 709–713.
- 15 Scrocco, E. and Tomasi, J., *Top. Curr. Chem.*, 42 (1973) 95–170.
- 16 Pople, J.A., Santry, D.P. and Segal, G.A., *J. Chem. Phys.*, 43 (1965) S129–S135.
- 17 Löwdin, P.O., *J. Chem. Phys.*, 18 (1950) 365–375.
- 18 Mulliken, R.S., *J. Chim. Phys.*, 46 (1949) 497–542.
- 19 Carbo, R. and Martin, M., *Int. J. Quant. Chem.*, 9 (1975) 193–214.
- 20 Daul, C. and Weber, J., *Chem. Phys. Lett.*, to be submitted.
- 21 Brown, D.A., Fitzpatrick, N.J. and McGinn, M.A., *J. Organomet. Chem.*, 293 (1985) 235–248.
- 22 Anderson, A.B., *J. Chem. Phys.*, 62 (1975) 1187–1188.
- 23 Howell, J., Rossi, A., Wallace, D., Haraki, K. and Hoffmann, R., *QCPE Bull.*, 11 (1979) 344.
- 24 Weber, J. and Roch, M., *J. Mol. Graph.* 4 (1986) 145–148.
- 25 Vaney, M.C., Surcouf, E., Morize, I., Cherfils, I. and Morron, J.P., *J. Mol. Graph.* 3 (1985) 123–124.
- 26 Weber, J. and Goursot, A., unpublished results.
- 27 Curphey, T.J., Santer, J.O., Rosenblum, M. and Richards, J.H., *J. Am. Chem. Soc.*, 82 (1960) 5249–5250.
- 28 Pavlik, I. and Subrt, J., *Coll. Czech. Chem. Comm.*, 32 (1967) 76–78.
- 29 Foster, M.S. and Beauchamp, J.L., *J. Am. Chem. Soc.*, 97 (1975) 4814–4817.
- 30 Lentzner, H.L. and Watts, W.E., *J. Chem. Soc., Chem. Commun.*, (1970) 26–27.
- 31 Lauher, J.W. and Hoffmann, R., *J. Am. Chem. Soc.*, 98 (1976) 1729–1742.
- 32 Davison, A., MacFarlane, W., Pratt, L. and Wilkinson, G., *J. Chem. Soc.*, (1962) 3653–3666.

- 33 Foster, M.S. and Beauchamp, J.L., *J. Am. Chem. Soc.*, 97 (1975) 4808–4814.
- 34 Werner, H., *Angew. Chem. Int. Ed.*, 22 (1983) 927–949.
- 35 Cook, D.J., Dawes, J.L. and Kemmitt, R.W.D., *J. Chem. Soc. A*, (1967) 1547–1551.
- 36 Dawes, J.L. and Kemmitt, R.W.D., *J. Chem. Soc. A*, (1968) 1072–1073.
- 37 Green, M.L.H., Pratt, L. and Wilkinson, G., *J. Chem. Soc.*, (1959) 3753–3767.
- 38 Khand, I.U., Pauson, P. L. and Watts, W.E., *J. Chem. Soc. C*, (1968) 2257–2260.
- 39 Sakaki, S., Kato, H., Kanai, H. and Tarama, K., *Bull. Chem. Soc. Jpn.*, 47 (1974) 377–383.
- 40 Hamilton, W.C., Klandermann, K.A. and Spratley, R., *Acta Crystallogr., Sect. A*, 25 (1969) S172–S173.
- 41 Ramdas, S., Thomas, J.M., Betteridge, P.W., Cheetham, A.K. and Davies, E.K., *Angew. Chem. Int. Ed.*, 23 (1984) 671–679.
- 42 Barthomeuf, D., *J. Phys. Chem.*, 83 (1979) 249–256.
- 43 Goursot, A., Fajula, F., Daul, C. and Weber, J., *J. Phys. Chem.*, 92 (1988) 4456.